Methane Airborne Detection Solution for the Oil & Gas Industry

Rev : 1

TELOPS inc.
100-2600 Ave Saint-Jean-Baptiste
Québec City, QC, Canada, G2E 6J5
www.telops.com

Table of contents

1 Introduction

The document *Description of Technology* provides a comprehensive overview of the Telops methane detection solution. To begin, an overview of the Hyper-Cam Airborne Mini is presented in **Section 2**, detailing its specifications and operational modes. Next, the scientific background of the technology is presented in **Section 3**. This section begins with an introduction to the basics of radiometry and signal creation. The signal passes through a Fourier-transform infrared spectrometer to measure the scene radiance. Then, the in-house detection algorithm based on the Generalized Likelihood Ratio Test and the quantification algorithm are introduced. **Section 4** outlines the overall workflow, starting with what a new partner can expect from the training and the preflight preparation. It then details the in-flight procedures, including hypercube creation and metadata handling. Moreover, the steps to follow post-flight are explained. **Section 5** presents the performance of the Hyper-Cam Airborne Mini, starting by explaining the impact of the spatial resolution and finally explaining an overview of the backbone of our solution, the detection limit. Finally, **Section 6** presents an overview of the limitations of the Hyper-Cam Airborne Mini.

2 System description

2.1 System overview

The Telops' methane airborne detection solution is based on our Hyper-Cam Airborne Mini (HCAM) device, a commercial airborne thermal infrared hyperspectral imaging system. This aircraft-based remote sensing system is a Fourier-transform infrared (FTIR) spectrometer that detects and quantifies methane emissions.

The HCAM system is designed in a compact two-unit assembly, the Control & Processing Box, or CPB, and the Sensor Head (see Figure 1). A field rugged laptop computer is used to control and monitor the HCAM system during an inspection flight. This design allows great flexibility in the positioning of system components, facilitating integration into different types of aircraft, from fixed-wing to helicopters. A few integration examples are shown in Figure 2.

In addition to the system components dedicated to airborne operation, the solution also includes a laptop computer for data processing after an inspection flight (details about the use of this processing laptop are given in section 4.4).

The Sensor Head is an Optical Head mounted on a compact stabilization platform. The Optical Head core component is an imaging Fourier-Transform Spectrometer operating in the Long-Wave InfraRed (LWIR) spectral band. In operation, the device provides 3D hyperspectral data cubes (i.e., hypercubes) with two spatial dimensions providing an image of the observed scene, and a third dimension providing the infrared spectrum of each pixel within the 2D image. Typical measurement time for one hypercube is 0.5 to 1 second, depending on flight conditions and device settings.

To ensure in-flight data integrity during measurement acquisition of each hypercube, the gyrostabilized mount on which the Optical Head sits provides roll, pitch and yaw stabilization, as well as pointing capability. At the optical entrance of the Optical Head, a fast-steering mirror provides an additional active mechanism to compensate for aircraft forward motion and maintain pointing toward the targeted inspection area. The system automatically adjusts to flight conditions (speed and altitude) to always maximize sensitivity and ensure optimal data collection. A GPS/INS module is integrated within the Optical Head to provide the required real-time compensation instructions to the stabilization platform. This GPS/INS module also provides timestamping and georeferencing metadata for each acquired measurement point along the flight trajectory. This metadata is saved within each hypercube image file, along with additional information such as an exhaustive list of system monitoring statuses, parameters for data processing and a wide variety of navigational information.

Figure 1: Picture of the Hyper-Cam Airborne Mini (HCAM).

Figure 2: The Hyper-cam Airborne Mini has been integrated and used in various types of aircraft.

Also incorporated within the Sensor Head is a 12-megapixel high-definition video imaging camera always pointing at the same location as the imaging spectrometer, providing a view in context of the scene to the operator in the visible spectral range. Each visible spectrum context image of the scene observed is also saved within each corresponding hypercube file.

Raw hypercubes with all corresponding metadata are directly generated within the Sensor Head onboard electronics, before being transferred to the CPB for storage on a solid-state drive and higher-level real-time processing, such as radiometric calibration, gas detection and gas identification. All raw and processed data are saved on the CPB over the entire duration of the flight. In addition, the CPB communicates to the Sensor Head the high-level mission parameters required for proper operation, such as geographical areas of inspection and other navigational parameters (like appropriate Digital Elevation Maps), as well as hyperspectral camera settings.

These parameters are taken from a mission plan established prior to the flight, which is executed and controlled by the HCAM operator through a field rugged Windows laptop computer.

When the HCAM inspects the ground, it autonomously selects where to point based on the currently active mission plan. As mentioned previously, the system uses its gyrostabilized mount and fast-steering mirror in order to maintain a fixed ground footprint for the duration of each acquired hypercube file. Once a file acquisition is completed, a new ground point is automatically selected at a new location in such a way that a predefined amount of overlap exists between consecutive hypercube (see Figure 3). The system offers great flexibility to meet various requirements for in-flight inspection and automatically adapts its acquisition parameters within a certain range during the flight, providing tolerance to variations in the aircraft attitude and trajectory, most notably the altitude.

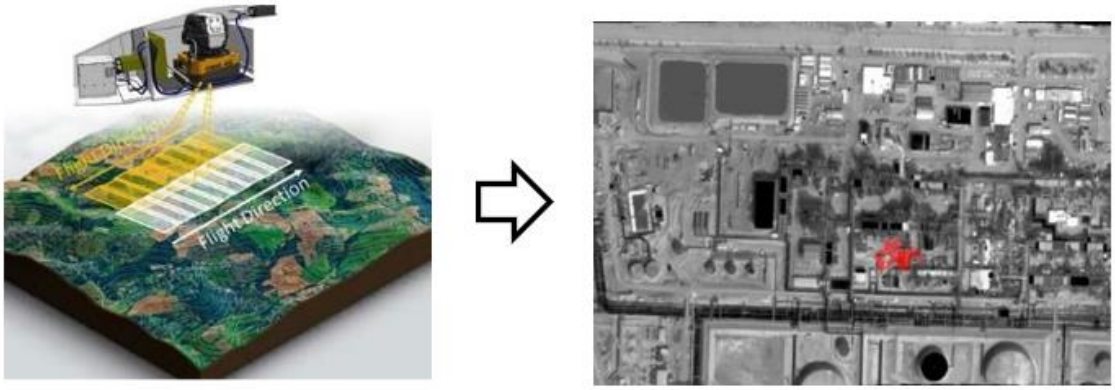

Figure 3: The HCAM acquires 3D images of the ground (2D spatial + 1 dimension spectral). In mapping mode, the system automatically ensures an overlap between each image to provide a 100% area coverage with no gap.

The in-flight imaging parameters such as *Track Width* and *Ground Sampling Distance (GSD)* of the HCAM instrument are dependent on flight altitude *Above Ground Level (AGL)*, the angular *Total Field Of View (TFOV)* and the *Instantaneous Field Of View (IFOV)*. These parameters are illustrated in Figure 4.

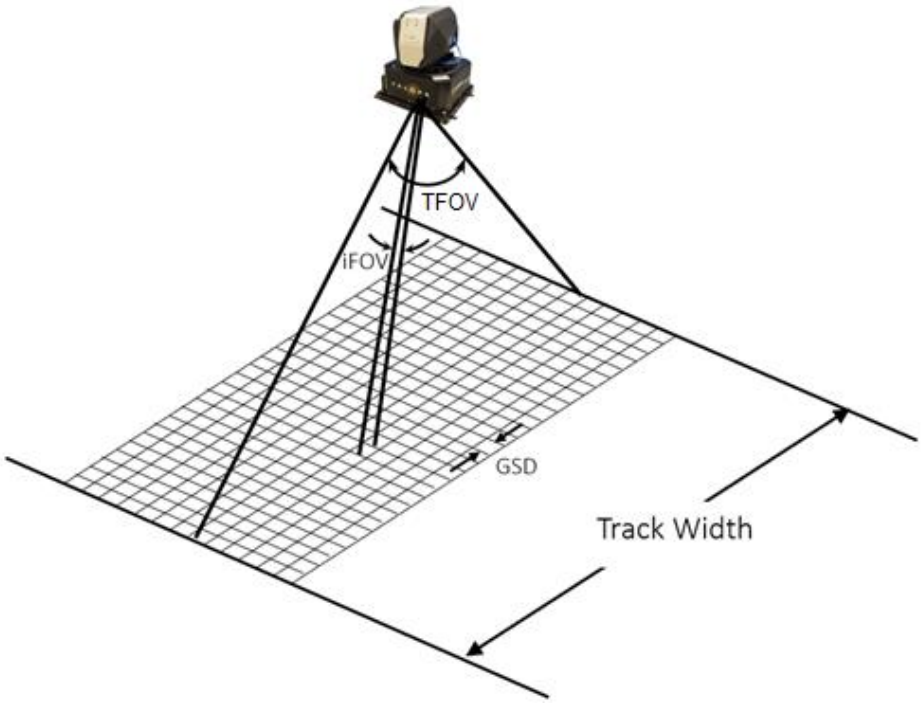

Figure 4: Image characteristics definition for the Hyper-Cam Airborne Mini

As shown in the above figure, the *Track Width* is the across-track size of the image on the ground, at a given *AGL*, as defined by the *TFOV* of the instrument. The *IFOV* is the field of view of a single pixel of the instrument, which defines the *GSD* at a given *AGL*. Table 1 provides values for in-flight imaging parameters for various flights *AGLs*.

Table 1: Track-width of the IR and visible images for various AGLs

Hyper-Cam Airborne Mini with 1x Fore Optic

	Infrared			Visible		
	GSD	Min Track Width	Max Track Width	GSD	Track-width	
FOV / AGL (m)	0.75	96	239	0.138	552	mrad
800	0.60	77	192	0.110	453	m
750	0.56	72	180	0.104	425	m
700	0.53	67	168	0.097	397	m
650	0.49	62	156	0.090	368	m
600	0.45	58	144	0.083	340	m
550	0.41	53	132	0.076	312	m
500	0.38	48	120	0.069	283	m
450	0.34	43	108	0.062	255	m
400	0.30	38	96	0.055	227	m
350	0.26	34	84	0.048	198	m
300	0.23	29	72	0.041	170	m
250	0.19	24	60	0.035	142	m
200	0.15	19	48	0.028	113	m

As shown in the above table, the IFOV of the Infrared imagery is 0.75 mrad, while the visible images have an IFOV of 0.138 mrad. Since the image width of the Infrared sensor can be adjusted from 128 to 320 pixels, the TFOV of the IR images can be adjusted from 96 to 239 mrad (5.5 to 13.7°). The visible camera generates images at fixed width of 4000 pixels, resulting in a TFOV of 552 mrad (31.6°). For instance, at an AGL of 350m, the infrared imagery would provide a GSD of 0.26m, with a track width that can vary from 34 to 84 meters.

Table 2 provides a summary of the Hyper-Cam Airborne Mini system specification for information purpose.

Table 2: Specification of the Hyper-Cam Airborne Mini

SPECIFICATION	VALUE
SPECTRAL RANGE *	7.4-7.52 to 12.42 µm (850 to 1330-1350 cm^{-1})
SPECTRAL RESOLUTION *	User adjustable: From 0.5 to 64 cm^{-1}
TYPICAL NESR	< 35 nW / (cm^2 sr cm^{-1}) @ 16 cm^{-1}
RADIOMETRIC ACCURACY	< 5 %radiance (over spectral range)
IFOV / TFOV	Infrared: 750 µrad / 13.7 x 11.0° Visible: 138 µrad / 31.6 x 23.2°
WEIGHT	< 24 kg
SIZE	CPB: 23 x 21 x 18 cm Sensor Head: 28 x 35 x 38 cm
MAXIMUM POWER CONSUMPTION	Steady state: < 340 W Maximum Peak: < 490 W
OPERATING TEMPERATURE	-10°C to +50°C
STORAGE TEMPERATURE	-20°C to +70°C

*Achievable maximum spectral resolution in flight depends on the minimum aircraft speed and is also function of the AGL. The Reveal Airborne Planner software manages the operable range within aircraft capabilities.

2.2 Operational Concepts

In the realm of pipeline and oil & gas infrastructure inspections, the Hyper-Cam Airborne Mini excels with its specialized corridor mapping mode. This mode uses strategic ground line placement during flight planning, allowing the HCAM to autonomously capture detailed scenes along predefined routes.

This mode makes the inspection very versatile, so the oil and natural gas owners/operators can use the corridor mapping mode for all their different facilities and pipelines.

Depending on the specific objectives of the campaign, it is crucial to optimally position the ground lines for inspection. For instance, when dealing with a straightforward pipeline, it is feasible to draw the ground lines over the pipelines for the aircraft to follow. In the example below (Figure 5), we observe that the aircraft can maneuver safely over the ground lines to achieve full coverage with a minimum of dead flight time.

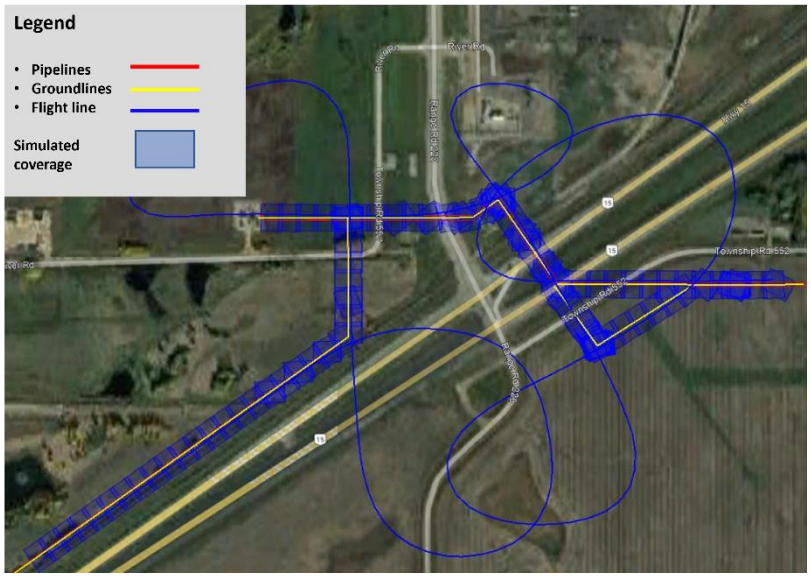

Figure 5: Example of a pipeline inspection using the HCAM in the corridor mapping mode

If the pipeline network is dense and spread out, as shown in the example below (Figure 6), or for the entire coverage of a site larger than the track width, it is possible (and recommended) to draw the ground lines in a "mapping" mode. This approach ensures full coverage and makes it easier for the pilot to manoeuvre the aircraft during inspection.

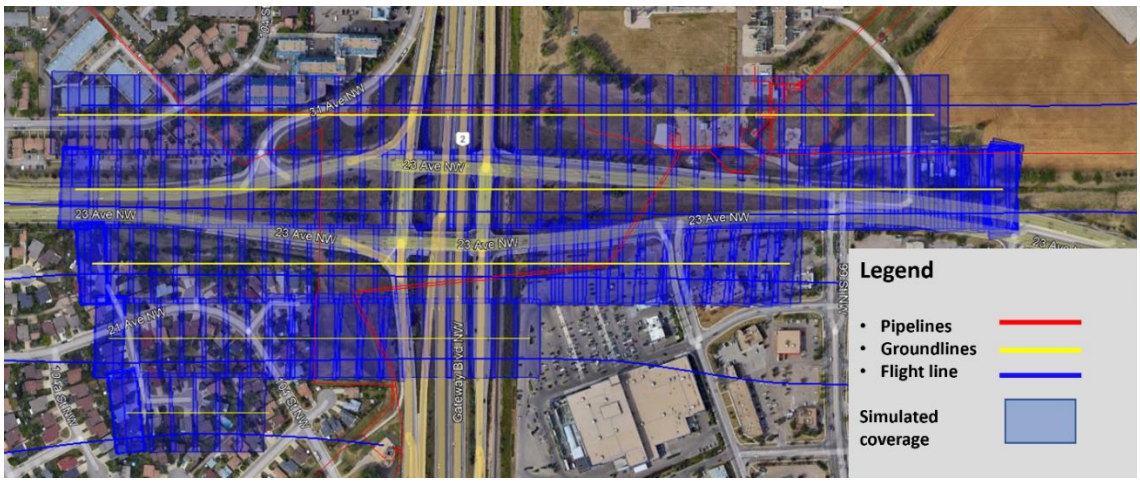

Figure 6: Example of a dense pipeline or an oil and gas facility inspection using the HCAM in the corridor mapping mode

3 Scientific background

This section details the mathematical and physical principles behind the technology. Detection of gases in the long-wave infrared band involves passively recording radiance emitted and absorbed by objects.

To detect methane, using passive measurements in the LWIR, two conditions must be met:

1. There must exist a thermal contrast between the background and the gas,

2. The atmosphere between the camera and the ground must be sufficiently transparent in the methane active region of the spectrum for the radiance signal to reach the camera aperture.

When these conditions are met, the presence of methane creates a spectral radiance signal that can be detected by the HCAM.

3.1 Radiometry

The total radiance measured by a pixel can be described using a radiometric transfer model (see Figure 7). Beginning at the ground, light (or radiance) from the atmosphere and surrounding objects is partly reflected by background objects, which also emit their own light (radiance). This emitted radiance is further absorbed and scattered by the atmosphere, which in turn emits additional radiance. If methane gas is present within the pixel's field of view, the emitted radiance interacts with it and is absorbed by the gas.

We can model this mathematically by a multilayer model in the form (Manolakis, 2014) :

$$L(\sigma)_{at\ sensor} = \left[L(\sigma)_{bkg}\tau(\sigma)_{plume} + L(\sigma)_{plume}\right]\tau(\sigma)_{atm} + L(\sigma)_{atm} \quad (1)$$

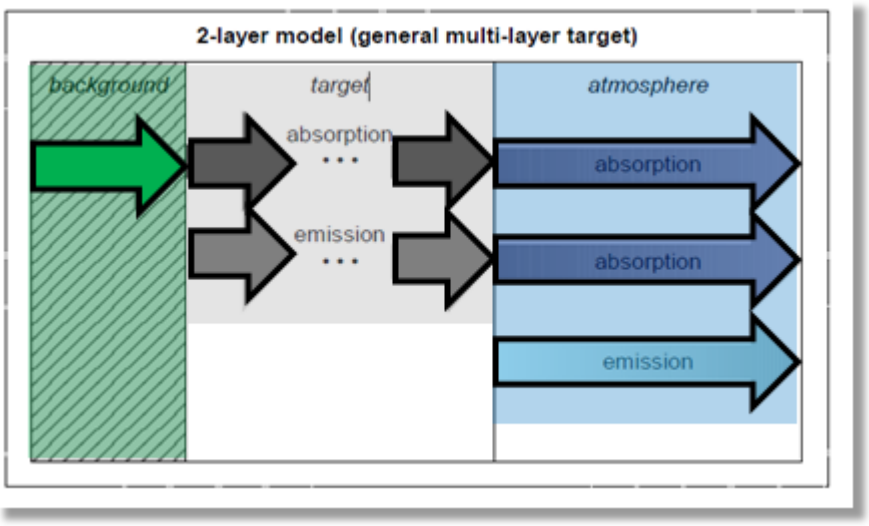

Figure 7 : 2 layers radiometric model

With L being the radiance, τ being the transmittance of the plume or the atmospheric layer and σ the wavenumber. The radiance for the atmosphere and plume layer is dependent on their spectral emissivity ε and temperature T, and can be expressed as follows (Andrews, 2010):

$$L_{layer}(\sigma) = \varepsilon(\sigma) * B(T) \quad (2)$$

$$B(T) = \frac{2hc^2\sigma^3}{e^{hc\sigma/k_BT}-1} \quad (3)$$

Where h is the Planck constant, c the speed of light, σ the wavenumber of light and k_B the Boltzmann constant.

The signal strength generated by a plume of gas is therefore driven by the thermal contrast between the ground (background under the gas) and the gas cloud.

$$(L_{with\ gas} - L_{without\ gas}) \propto GasQuantity * (T_{plume} - T_{bkg}). \quad (4)$$

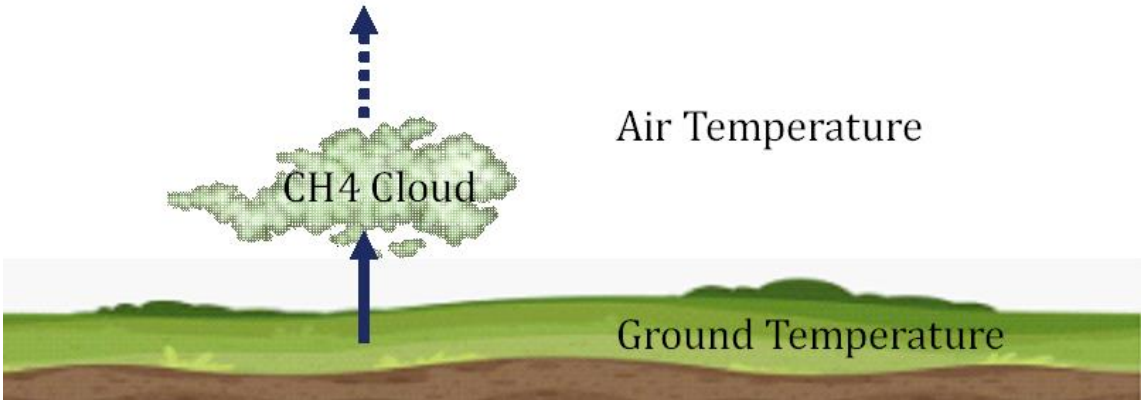

Figure 8: Example of the signal from the ground passing through a cloud of methane.

Note that the signal can be either positive or negative. When the gas temperature is higher than the background temperature, the presence of the gas generates a positive signal called "emission." In the opposite situation, i.e., the gas temperature is lower than the background, the gas generates a lower signal relative to the background radiance and this is called "absorption" signal. Both cases are equally detectable.

The emissivity ε(σ) of each gaseous layer can be determined by the thickness of the layer, the concentration, and the absorption spectral signature of each gas. The absorption spectral signature of gases is calculated based on Hitran line by line database 2020 (Gordon, 2022) using Beer's law (Manolakis, 2014).

3.2 At-Sensor Radiance Measurement

Spectral measurement of at-sensor radiance is performed via a Fourier transform spectrometer. Each pixel of the instrument's Focal Plane Array (FPA) records an interferogram which is then converted by Fourier transform into a complete raw spectrum of the acquired light, providing the intensity at each wavelength (λ). Calibration of this raw measurement to radiance units (W/(m^2*sr*cm^{-1})) is achieved using known high-emissivity surfaces (blackbodies) at known temperatures, as their radiance depends solely on their temperature according to Planck's law. The Hyper-Cam Airborne Mini includes two of these reference blackbodies (called Internal Calibration Targets), allowing for frequent characterization of the system gain and offset through measurements of these blackbodies. These calibrations are performed automatically by the system when required.

Using these two measurements, the radiometric gain and offset are computed as follows for each pixel (Revercomb, et al., 1988):

$$G(\lambda) = \frac{M_2(\lambda) - M_2(\lambda)}{L_2(\lambda) - L_1(\lambda)} \quad (5)$$

$$O(\lambda) = M_2(\lambda) - G(\lambda) * L_2(\lambda) \quad (6)$$

Where G is the gain and O the offset of the instrument, M is the measurement and L the theoretical radiance emitted by the reference surfaces.

The spectral radiance is then calculated from a scene measurement with

$$L_{measured}(\lambda) = \frac{M(\lambda) - O(\lambda)}{G(\lambda)} \quad (7)$$

3.3 Gas Detection

Using the radiance of each pixel, gas detection is done using the Generalized Likelihood Ratio Test (GLRT) (Manolakis, 2000). This test computes the probability that methane is present in each pixel using the formula:

$$GLRT(x) = \left[\left(\frac{x^T(P_b^{\perp} - P_S^{\perp})x}{x^T P_S^{\perp} x}\right) + 1\right]^{L/2} \quad (8)$$

Where x is the pixel spectrum, L the number of bands in the spectrum, $P_b^{\perp}$ the projection operator on the background subspace, $P_S^{\perp}$ the projection operator on the background subspace extended with the target (methane) signature.

The background subspace is constructed from a principal component analysis of a set of pixels which are unlikely to have been polluted by the target.

The GLRT score from this equation is computed for each pixel. The higher the score, the higher the probability that methane is present in the pixel. The GLRT score can be shown in an image format, called a score map, along with other information. The final detection report is verified and confirmed by a trained professional (Telops' analysts).

3.4 Gas Quantification

3.4.1 ppm*m Quantification

To quantify the amount of gas in each pixel, an algorithm developed by Onera is used (Foucher, 2020). The gas transmittance is computed as follows:

$$\tau_{gas} = 1 + \frac{L_x - L_{ref}}{L_{ref} - L_{atm} - \tau_{atm} B(T_{gas})} \quad (9)$$

Where L_x is the measured radiance for each pixel. The background radiance L_{ref} is reconstructed using principal component analysis (Idoughi, 2016). The atmospheric contribution L_{atm} and τ_{atm} are calculated using the ISAC method (Young, 2002). The temperature of the gas T_{gas} is considered equal to the temperature of the air at ground level which is determined using meteorological data (see next section).

We can deduce the amount of gas, in ppm*m, required to obtain a layer transmittance of τ_{gas} by inverting the exponential absorption equation using the theoretical methane absorbance from Hitran (Gordon, 2022).

3.4.2 Flow Rate Quantification

Using the ideal gas law, it is possible to convert the ppm*m value in grams per pixel. The equation can be expressed as:

$$PV = nRT = nK_B N_A T \quad (10)$$

Where P is the pressure of the gas (in Pa), V is the volume occupied by the gas (in m^3), T is the temperature of the gas (in K), K_B is the Boltzmann constant (in J/K), N_A is the Avogadro constant (mol^{-1}) and n is the amount of

substance of gas (in mol). The above equation can be expressed as the molar volume V_m, describing the volume occupied by one mole of substance:

$$V_m = \frac{K_B N_A T}{P} \tag{11}$$

Regarding the quantification map, for each pixel in the image, we have its methane content in ppm*m. It is then possible to convert it in mass (g) by using the following equation:

$$g = \frac{M \cdot ppm*m \cdot {}^{1}/_{1e^{-6}}}{V_m} A_{px} \tag{12}$$

With M being the molar mass (in ${}^{g}/_{mol}$) and A_{px} the pixel size (in m^2).

Knowing the length L (in m) of the plume along the wind direction and using the wind speed V (in ${}^{m}/_{s}$), it is possible to calculate the flow rate FR :

$$FR = \frac{g}{L} \times V \tag{13}$$

Here is an example of a typical quantification map in g (see Figure 9). It is also possible to see the length L of the plume (red line) on this figure.

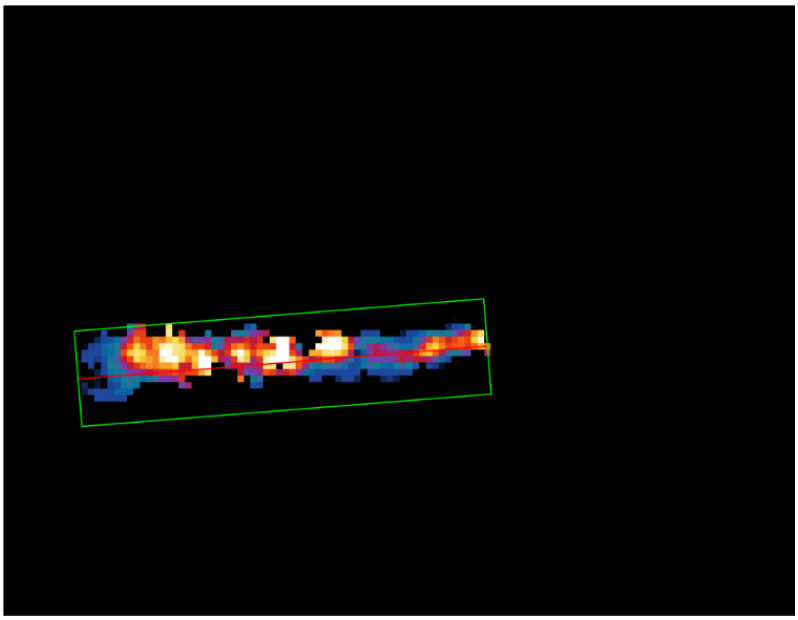

Figure 9: Example of a quantification map with the length L of the plume (in red)

4 Workflow

This section discusses the overall workflow, from system installation and inspection preparation to a detailed description of what the Telops solution brings to oil and natural gas owners/operators. Telops collaborates with flight partners. These partners usually act as prime contractors, engaging with oil and natural gas owners/ operators who request inspections for methane releases. Telops supplies the Hyper-Cam Airborne Mini (HCAM) to these partners. The partners are responsible for providing an aircraft and qualified personnel (such as a pilot and HCAM operator) to install the HCAM, planning and executing inspection flights, and transferring

acquired data to a processing PC. Telops manages post-flight data processing and prepares materials for deliverables. The partner is responsible for providing oil and gas owners/operators with final inspection reports and any customized supporting files requested by them.

The following subsections present in detail the steps of the workflow.

4.1 Training

Each new partner gets training from Telops on the operation of the system. The training includes everything needed from the basic measurement principle to the operation and the data validation:

- An overview presentation
- Demonstration of the system's functionality
- Creation of the Mission files including the inspection ground lines
- System interface definition and integration into an aircraft
- Support for a flight test
- Post-flight data transfer and processing, including inspection statistics

4.2 Pre-flight preparation

The first step of the workflow is the preparation of the inspection plan. The oil and natural gas owners/operators provide a list of sites or equipment to be inspected. It can be in the form of a KML/KMZ file listing the discrete GPS locations of the equipment to be inspected or showing the areas of the sites or the pipeline to be inspected. Based on the locations of the items to be inspected, the items are grouped into smaller subgroups and a flight plan is prepared for each subgroup. Depending on the detection limit requested by the owners/operators, the basic flight and instrument parameters are determined; they consist of the flight altitude (AGL: Above Ground Level), the flight speed and the inspection track width. A prediction tool is provided by Telops to help the partner to select these parameters and to choose the type of aircraft to use (for slower flight speeds, a helicopter might be needed). Figure 10 below presents the detection limit tool user interface (UI):

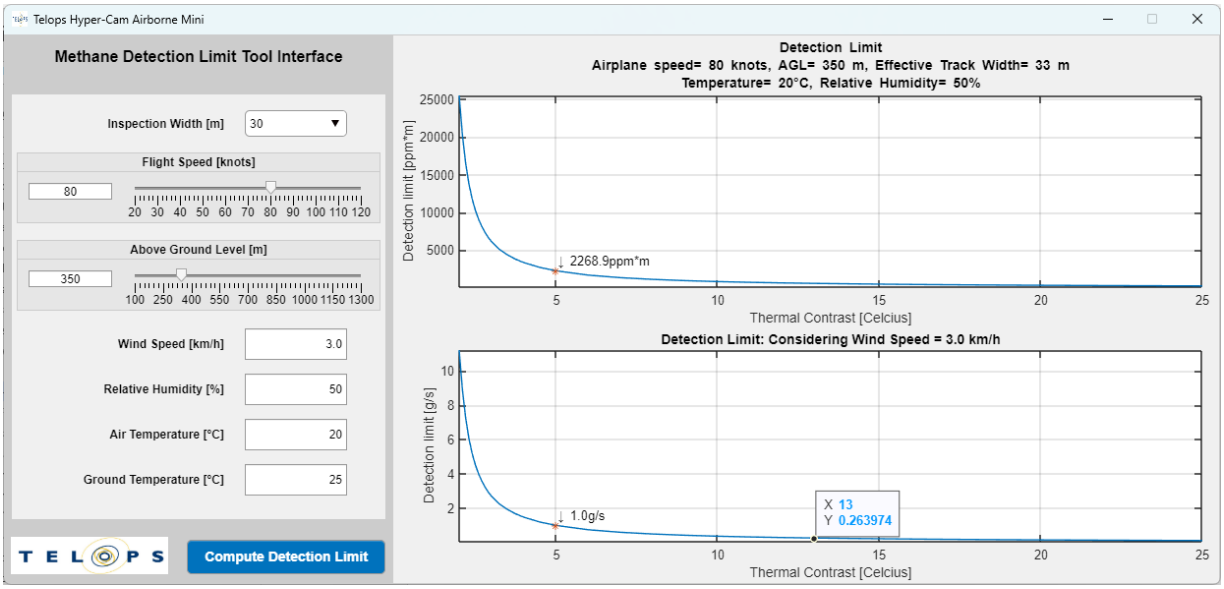

Figure 10: Methane Detection Limit Tool UI

One can see the example for a flight at 350m AGL, 80 knots and with an inspection track width of 30m: the 90% POD limit is 1g/s for a scene with 5°C of thermal contrast and is 0.26g/s (1kg/hr) with a thermal contrast of 13°C.

Once the flight plan is set and the flight lines determined, the next step is to draw the inspection ground lines (IGLs) over the sites or equipment to be inspected, with the same orientation as the flight lines. The IGLs are used by the HCAM to automatically adjust and stabilize the centre of the image and record data as the airplane flies by. They are the centre of the inspection corridors where the HCAM captures hyperspectral data in corridor mapping mode. Figure 11 below shows an example of a site with 2 IGLs (yellow lines):

Figure 11: Example of Inspection Ground Lines (IGL) in yellow over a site to be inspected

When the width of a site to be inspected is larger than the HCAM track width, parallel IGLs need to be created and the spacing between these IGLs is generally chosen to give a 10% overlap between each track. Under these conditions, a site is fully measured with 100% spatial coverage at a resolution corresponding to the GSD (Ground Sampling Distance) as determined by the AGL (seeTable 1). The list of all IGLs coordinates has to be saved in a KML file. Using the Telops' Reveal Airborne Planner software, a mission file is prepared. The IGLs are imported into the mission from the KML file.

Here is the list of things to do before a flight.

- The Mission file must be completed and saved on the in-flight Laptop. The file will be transferred by the HCAM operator to the system at the start of the flight.
- Look over the weather forecast to determine the best time to fly in conjunction with the *Detection Limit Tool*
- The HCAM has to be installed in the aircraft and the flight plan ready.

4.3 In-Flight Operation

At the beginning of the flight, the HCAM operator uploads the mission file into the camera head. After a warm-up period of 15 minutes, it is recommended to request a radiometric calibration measurement. The HCAM operator monitors the feedback from the instrument during the flight. The key feedback are the status of the radiometric calibration, the progress on the inspection areas, the current ground temperature (used to estimate the thermal contrast) and the flight parameters (mainly to verify they are at the planned values). Note that the HCAM automatically adjusts itself to ensure full coverage of the scene. Detection limits are impacted either positively or negatively depending on these adjustments.

During the flight, the HCAM automatically records calibration data whenever needed to achieve the best possible radiometric accuracy. The HCAM's optical head automatically points to the nearest inspection ground line in the

selected mission file. Scene acquisition is automatic when an IGL is tracked. The system automatically generates the radiance hypercube, and the methane detection algorithm is applied on each scene radiance hypercube with a conservative threshold so that only a significant potential leak will trigger a positive detection report. This process is executed in real-time for each scene, and the HCAM operator has access to all those reports real-time via the in-flight laptop.

For each scene, there is metadata stored in each hypercube. This metadata includes the visible image, an accurate timestamp from the GPS, accurate geo-localisation of the images, ID of the calibration file used to compute the radiance, system internal temperatures, GPS/INS data, and much more.

4.4 Post-Flight

After the flight, the HCAM operator removes the SSD from the CPB. The SSD contains all the data acquired during the flight. The SSD is connected to the processing Laptop along with an external HDD for archiving the data. The Processing Laptop must be connected to the internet.

Using the Telops' software *InspectionStats*, a back-up copy of all the data is created on the archive disk and the inspection report is generated. The Telops Team recommends to the partner to make an extra backup copy of the flight data. The *InspectionStats* tool gets the weather information for each scene (with the timestamp and GPS location) from a web-based service (Business API Package) Meteomatics (www.meteomatics.com) which provides comprehensive meteorological data and weather information services tailored to diverse industries. Meteomatics is used to get the air temperature and wind speed at the ground level at the exact location and time of the inspection measurement. This information is used to compute the thermal contrast at the time of the inspection which is used to calculate the detection limit in ppm*m and the wind speed to convert the detection limit in release rate (g/s). These detection limits are the ones reported in the Inspection Statistics report. The *InspectionStats* tool generates the Inspection Statistics Report (Deliverable Package #1) which is used to assess the quality of the inspection and to decide on the need to re-inspect or not the flown areas.

With a remote desktop software connected to the Processing Laptop, the Telops Team takes over the data processing, while the partner is ready to continue the inspection with the HCAM. Here are the main points of the postprocessing done by the Telops teams:

Using our postprocessing algorithm, we generate a methane detection score map for each scene hypercube. It is also at this step that are generated all the image files for the Deliverable Package #2. A one-page report is created using the spectral radiance, visible image, the weather data and the different methane detection score map then each scene are ranked on the likelihood of detection. An analyst from the Telops Team analyses each scene using the one-page report and ranking to filter out the scenes where the methane detection score is very low and keeping all the ones with potential detections (either positive or negative).

The analyst's selected scenes (hypercubes) are then transferred from the remote processing Laptop to Telops internal network via Microsoft OneDrive. The remaining steps of the postprocessing are done on local computers at Telops. A thorough analysis is done for each scene to eliminate what appears as false positive detection. During that step, each detection accepted as a positive detection is attributed a confidence level (high or low) by the analyst. The methane quantification algorithm is applied on each positive detection hypercube to create the quantification map in ppm*m. At this step, each pixel of the IR hypercube gets a quantity of methane (in grams) by the conversion of the ppm*m using the known pixel footprint area computed from the AGL in the metadata (coming from the GPS/INS). The final step consists of estimating the release rate using the mass map and the wind speed. Complete detection reports are generated along with quantification estimates and other information. These reports constitute the Delivery Package #3.

Note that any data transfer done between the remote processing Laptop and the Telops team passes through Microsoft OneDrive. This process is repeated for each flight. Feedback by the Telops team and discussion with

the partner (HCAM operator) occurs on a regular basis for system supports and interpretation of the Inspection Statistics report for recommendation on optimal flight time (to achieve better thermal contrast).

The oil and natural gas owners/operators can expect to receive 3 different packages in 3 different timelines (see appendices for a more detailed version):

Table 3: Summary of the different delivery packages

Package	Delivery Time	Description
1	Within 24 hours	Inspection Statistics report
2	Within 2 days	Visible image of each scene and georeferenced IR and Visible images
3	Within 2 weeks	Detection Reports (Georeferenced IR, Visible Image and plume)

All the packages are delivered to the partner via a shared drive in Microsoft OneDrive. The partner is responsible for the deliveries of all the packages to the owners/operators.

Once the campaign is completed, the entire system including the archive disk are shipped to the Telops headquarter (Quebec City). Upon reception of the system, a rigorous demobilization procedure is done by our Team. The system goes in a series of tests to be ready for the next campaign and all the data is transferred and archived into our dedicated workstation. Telops keeps an archive copy of the flight data and all the postprocessed results for a minimum of 2 years after the inspection campaign.

5 Performance

The Hyper-Cam Airborne Mini is a commercial thermal infrared hyperspectral imager manufactured and sold by Telops inc. The mini version has been introduced into the market in 2021, replacing the original Hyper-Cam Airborne launched in 2012. Each system is fully tested as part of the manufacturing process and a compliance test report is generated. Table 4 presents the key specifications of the Hyper-Cam Airborne Mini tested in production and having a direct impact on the system performance for methane detection, localization and quantification.

Table 4: Key specifications for the Hyper-Cam Airborne Mini

Parameter	Units	Value
NESR (Noise Equivalent Spectral Radiance)	$\frac{nW}{cm^2 \cdot sr \cdot cm^{-1}}$	< 35
Radiometric Accuracy	% of radiance	< 5
Absolute Geolocation Accuracy	m	< 5

The following subsections present in detail the spatial resolution and geolocation accuracy as well as the 90% POD methane detection limit of the HCAM.

5.1 Spatial Resolution

The Hyper-Cam Airborne Mini has 2 imaging channels (see section 2.1), namely the hyperspectral infrared and the visible. The thermal infrared hyperspectral imager has a square iFOV of 750µrad providing a pixel footprint on the ground (GSD) of 26cm when flying at 350m AGL. The Ground Sampling Distance (GSD) for other AGLs are presented in Table 1. For the visible image, the iFOV is 138µrad, giving a pixel footprint on the ground of 4.8cm

at 350m AGL. Using this high-resolution imagery, the relative position of a detected methane cloud to the ground equipment can easily be determined. Since the presence of methane is determine for each pixel of the infrared image, the methane localization is determined with a resolution better than 0.5m for any AGL below 650m.

An example of the achieved resolution and accuracy of the geolocation is presented in the following figures (Figure 12 and Figure 13).

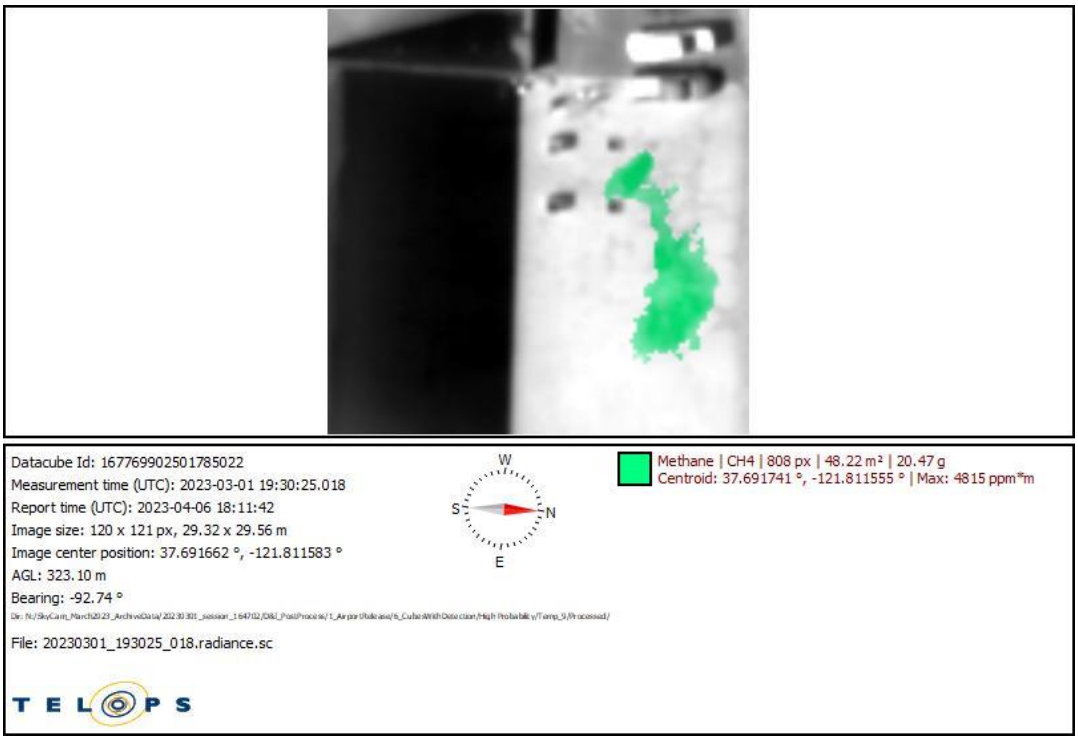

Figure 12: Example of detection report where the position of the methane cloud is clearly determined in the infrared image and the GPS coordinates of the centre of mass are given.

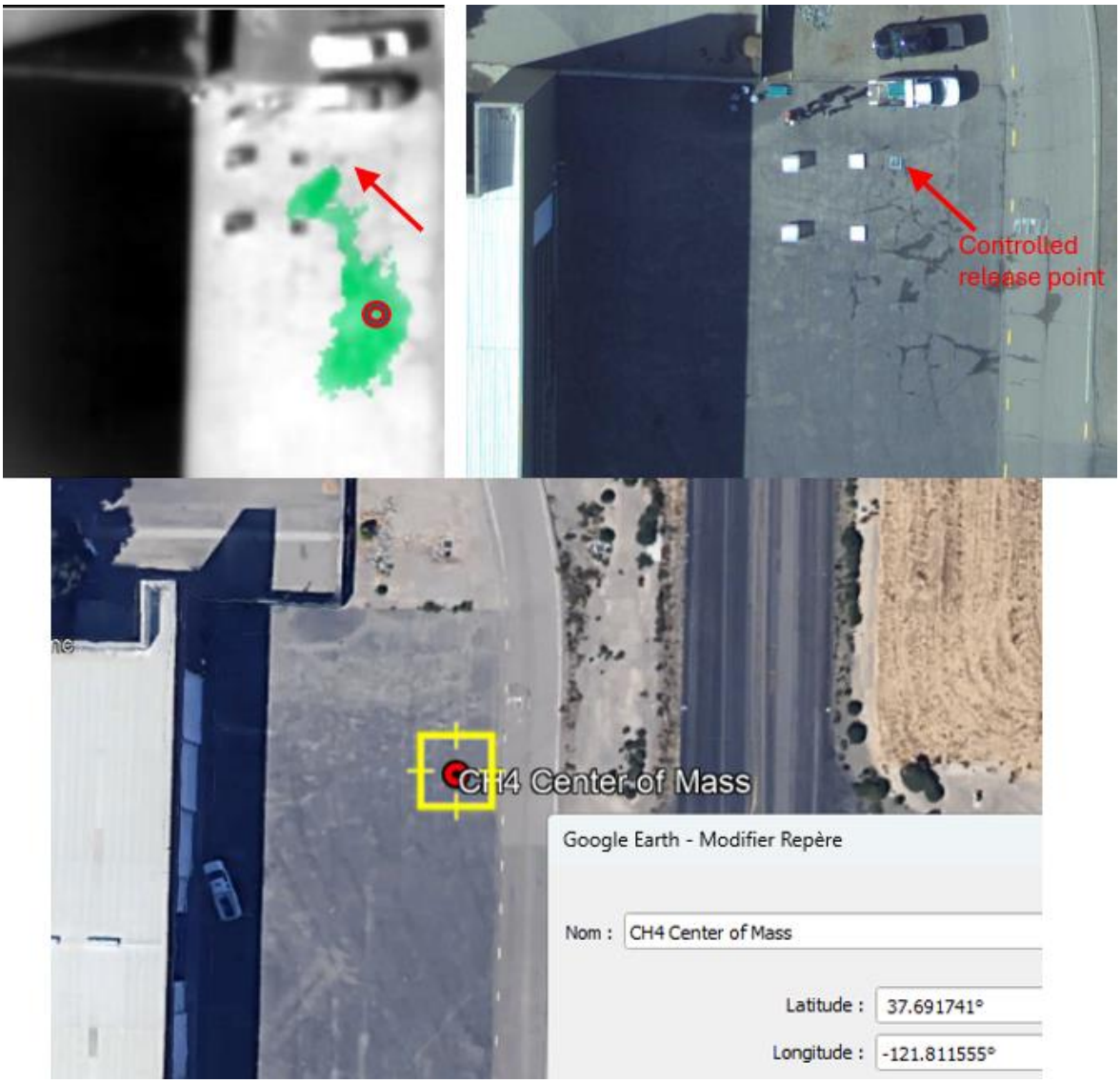

Figure 13: Emission source located within 0.5m using the high-resolution imagery of the Hyper-Cam Airborne Mini. Top-left image is the infrared image where pixels containing the methane are coloured in green. Top-right image is the visible image acquired at the same time as the infrared hypercube. The controlled release point is indicated. The bottom image is from Google Earth with the marker at the GPS coordinates of the centre of mass as reported in the detection report.

Referring to Figure 13, one can appreciate the high-resolution imagery which enables the location of the emission source with a resolution better than 0.5m. Using the 323m AGL from the report, the infrared image resolution (GSD) is 24cm and the visible image resolution is 4.5cm. It is worth to know that the 2 imaging channels of the Hyper-Cam are geometrically calibrated at the manufacturing time for remote sensing photogrammetry. This geometric calibration allows the use of direct georeferencing to get the exact location of any pixel of the image (Bäumker, 2002). Due to the variations of the received GPS signal and the number of satellites at any time, the absolute geolocation accuracy varies between 0.5 to 5m. Nevertheless, the use of the high-resolution images and the relative position of the objects within the image allows to reach a location accuracy of the methane on the order of the pixel footprint (GSD).

5.2 Methane Detection Limit

In this section, we present the theory used to determine the methane detection limit of the Hyper-Cam Airborne Mini and the results of experimental tests using controlled releases (both blind and non-blind). The tests demonstrated the actual methane detection limit of the system and validated the detection limit model.

5.2.1 Detection limit model

Telops has developed a detailed detection limit model for the Hyper-Cam Airborne Mini. Essentially, the model is divided into 3 parts:

1) Calculation of the at-sensor radiance signal coming from the scene,
2) Calculation of the methane concentration map from a constant leak rate and a plume model,
3) Calculation of the HCAM noise level.

5.2.1.1 At-sensor radiance signal modeling

The calculation of the at-sensor radiance is done using a multi-layer scene model where the background, the presence of the methane cloud and the atmospheric transmittance are taken into account in a radiative transfer model. This has been presented in section 3.1 and the basic theory is well covered in (Manolakis, 2014). This first part of the model calculates the radiance produced by the presence of the methane cloud as a function of

- the concentration path length of the methane (in ppm*m),
- the thermal contrast between the methane and the background,
- the atmospheric transmittance which is function of the AGL and the humidity level.

Figure 14 presents an example of the spectral radiance signal received at the input of the camera for a thermal contrast of 5°C at an AGL of 350m in a summer wet atmosphere. The signal level is presented for various methane quantity from 10 to 50000 ppm*m.

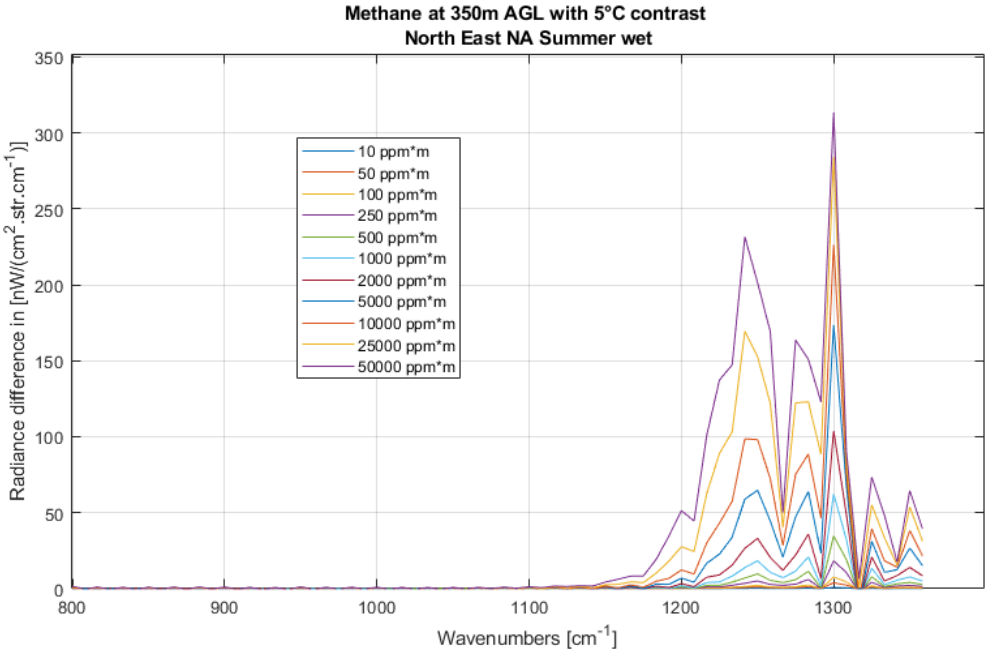

Figure 14: Example of the at-sensor radiance signal produced by the methane

5.2.1.2 Methane plume model

The second part of the detection limit model is the plume model. This part of the detection limit model is only needed when one wants to convert the detection limit in ppm*m for the HCAM pixels into a release rate. We are using the Pasquill-Gifford Gaussian model to get the gas concentration downwind a release point (Hodgkinson, et al., 2006).

Since the HCAM images the plume, each pixel sees a different concentration of methane. We sort the concentrations per pixel and make the conservative assumption that for detection, at least 10 pixels of the HCAM must have their detection limit above the concentration produced by the plume dispersion. This gives us the concentration coefficient needed to convert the detection limit in ppm*m into the release rate in g/s. This coefficient is presented in Figure 15 where one can see that the seen concentrations by the pixels get lower as the AGL is increased.

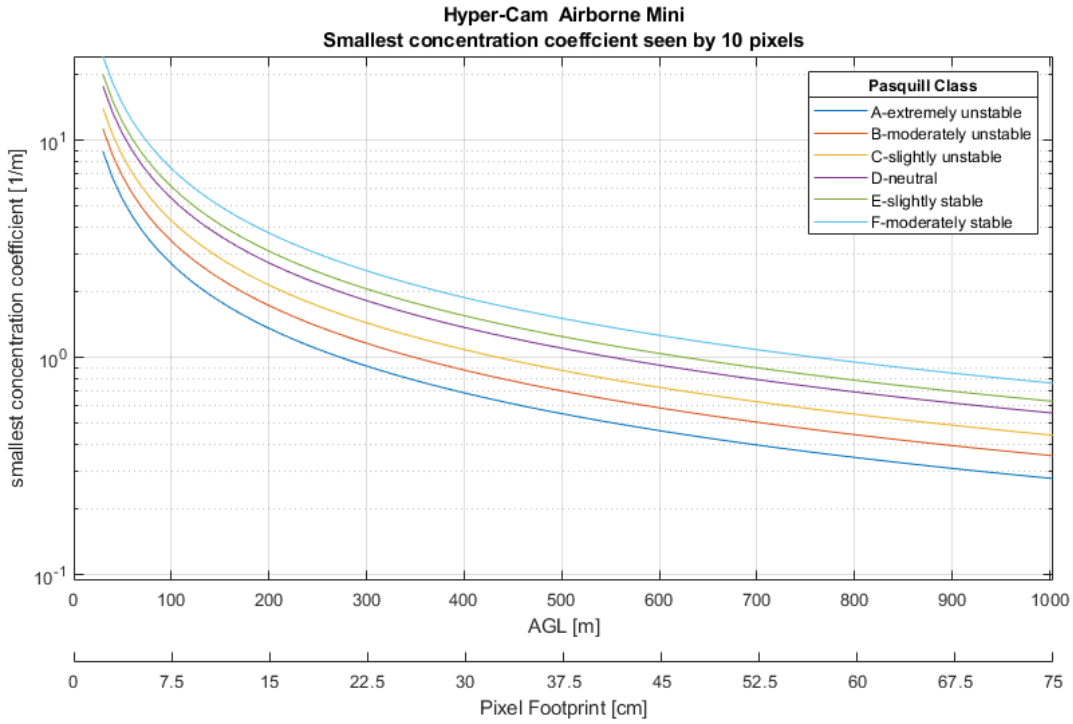

Figure 15: Concentration coefficient from the Gaussian plume model for the HCAM as a function of the AGL

Using this calculated smallest concentration coefficient, the complete equation to convert the detection limit in ppm*m into release rate is presented here:

$$\text{leakRate}\left[\frac{g}{s}\right] = \frac{\text{CH4coeff}\left[\frac{g}{ppm \times m^3}\right] \times \text{gasConcentration}\,[ppm \times m]}{\text{concentrationCoeff}\left[\frac{1}{m}\right]} \times \text{windSpeed}\left[\frac{m}{s}\right]$$

where the wind speed is explicitly shown and the CH4coeff (6.534×10^{-4} g/(ppm × m^3)) is used to convert the methane concentration from g/m^2 to ppm*m.

5.2.1.3 Hyper-Cam Airborne Mini noise level

The third part of the detection limit model is the Hyper-Cam Airborne Mini noise level. The NESR (Noise Equivalent Spectral Radiance) is the noise of the camera expressed in units of at-sensor radiance [$nW/(cm^2 \cdot sr \cdot cm^{-1})$]. This commercial product has a well-known and measured NESR. For the detection limit calculations, we are using the NESR from the specification of the product even if each built camera is tested separately and has a NESR smaller than the product line specification.

The NESR value has a dependence on the measurement time, i.e. the duration of the scene observation. When the HCAM is operated in mapping mode, the duration of the measurement is automatically adjusted to get a complete coverage of the ground with 10% overlap between each image. The duration depends on the flight speed and AGL. The actual duration of a scene measurement is measured for each scene and included in the metadata of the hypercube and used for the calculation of the actual detection limit for that scene. In the methane detection limit tool, the duration is derived from the planned flight speed and AGL.

5.2.1.4 Use of the detection limit model

The model combines the 3 parts explained above to determine the quantity of methane needed to produce a radiance signal higher than twice the NESR level as measured by the 10th ranked pixel. Our detection limit model is used in 2 different tools in our standard commercial inspection service. First, we have the detection limit prediction tool. This tool is used before an inspection job to determine the operating parameters (flight speed, AGL and instrument track width) to meet the oil and natural gas owner/operator detection limit requirement. Once the operating parameters selected, the tool is also used to predict when the weather should be fine to fly (thermal contrast and wind speed forecasts). Here is a screenshot of our tool:

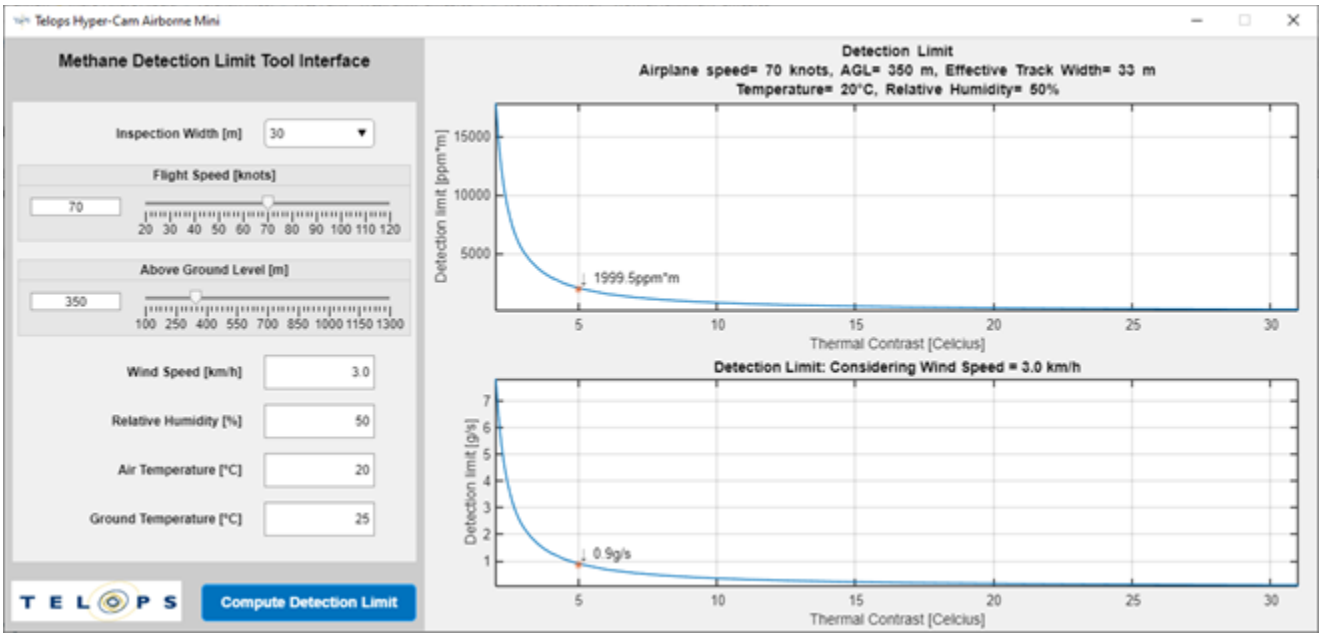

Figure 16: Screenshot of the Methane Detection Limit tool

In Figure 16, one can see that the detection limit is presented in ppm*m (top graph) as a function of the thermal contrast. The key input values are presented in the title above the top graph. The conversion into release rate is presented in the bottom graph where the wind speed is used as an input as well as the plume model presented in section 5.2.1.2 above.

During the flight, the HCAM computes the actual ground temperature for each scene hypercube and gives this value as feedback to the HCAM's operator. The HCAM's operator can then use the knowledge of the current air

temperature at the ground level from its preferred weather website and determine the actual thermal contrast to determine if it is worth continuing the inspection flight using the rule of thumb that a 3-degree contrast or higher is preferable. Figure 17 shows a screenshot of Reveal Airborne (the software used by the HCAM's operator) where the scene temperature is shown (labeled "Ground Temp").

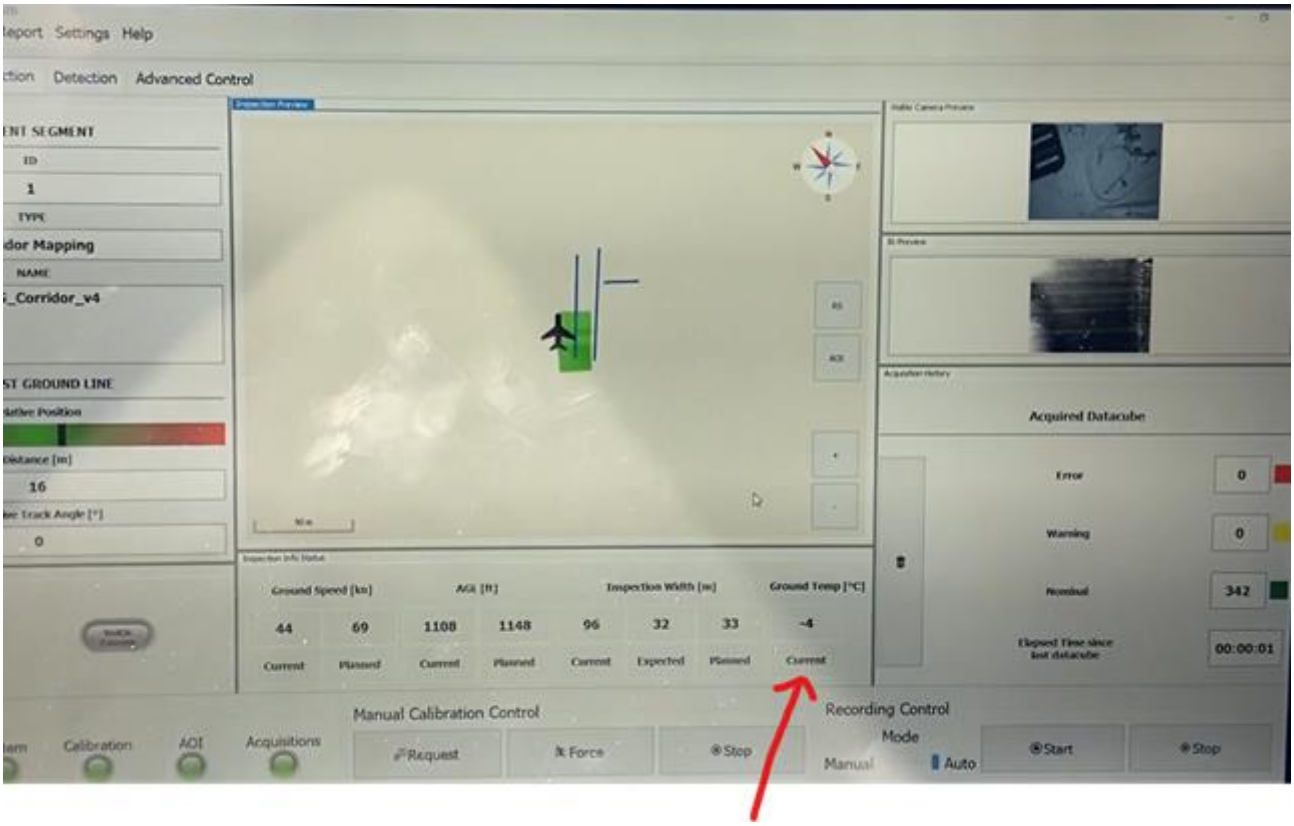

Figure 17: Screenshot of Reveal Airborne showing the ground temperature reported in real-time

The tool InspectionStats is also using the detection limit model. Just after the flight, the tool InspectionStats is run, and the HCAM's operator immediately gets the detection limits for every measured scene. The HCAM's operator can decide if a site needs to be revisited if the obtained detection limit is not within the customer requirements. Figure 18 gives an example of the calculated detection limit for a scene.

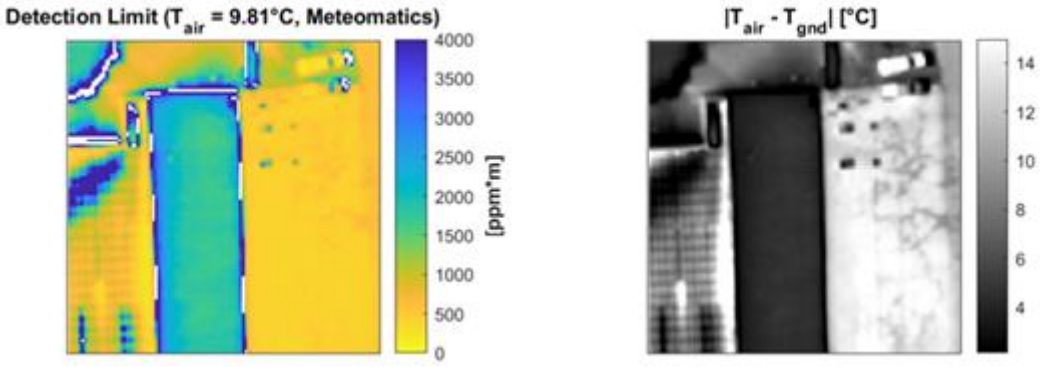

*Figure 18: Example images of thermal contrast and calculated detection limit. The right figure shows the thermal contrast calculated for each pixel and the left figure presents the resulting detection limit in ppm*m.*

One can see that each pixel has its own thermal contrast and a corresponding detection limit. The median value is used to attribute a single value for the detection limit, and this is what has been tested experimentally to verify the performance model.

Finally, in the final inspection report, the calculated detection limit is presented for each site inspected using again the detection limit model and the metadata from the scene measurements. A sample page report where one can see the detection limit for the site inspected is presented in Figure 19.

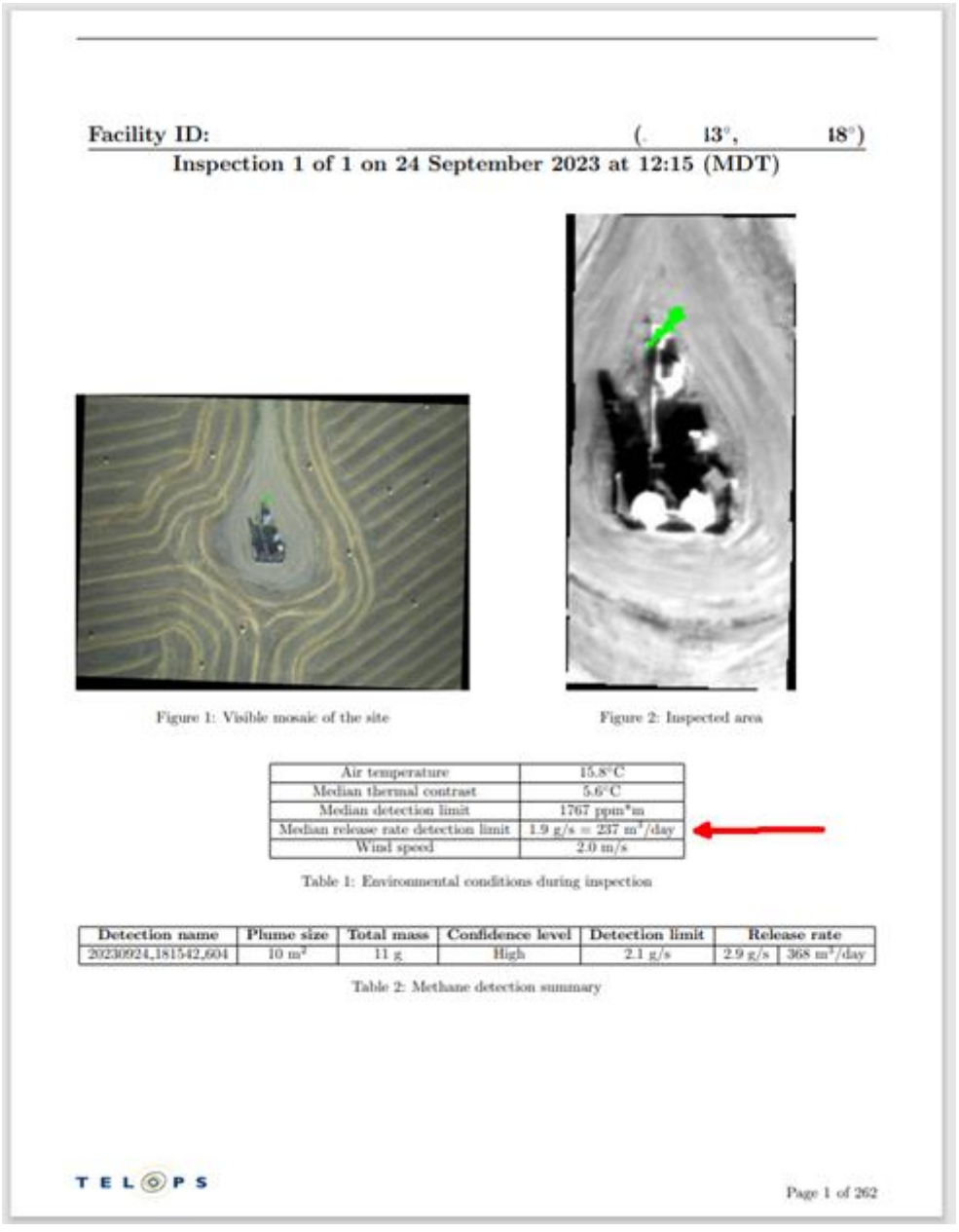

Facility ID: (13°, 18°)

Inspection 1 of 1 on 24 September 2023 at 12:15 (MDT)

Figure 1: Visible mosaic of the site

Figure 2: Inspected area

Air temperature	15.8°C
Median thermal contrast	5.6°C
Median detection limit	1767 ppm*m
Median release rate detection limit	1.9 g/s = 237 m³/day
Wind speed	2.0 m/s

Table 1: Environmental conditions during inspection

Detection name	Plume size	Total mass	Confidence level	Detection limit	Release rate	
20230924_181542_604	10 m²	11 g	High	2.1 g/s	2.9 g/s	368 m³/day

Table 2: Methane detection summary

TELOPS

Page 1 of 262

Figure 19: Sample page of the inspection report where the actual detection limit for that site is highlighted

When there is a detection, the detection limit for the specific plume area is also documented as shown in Figure 20.

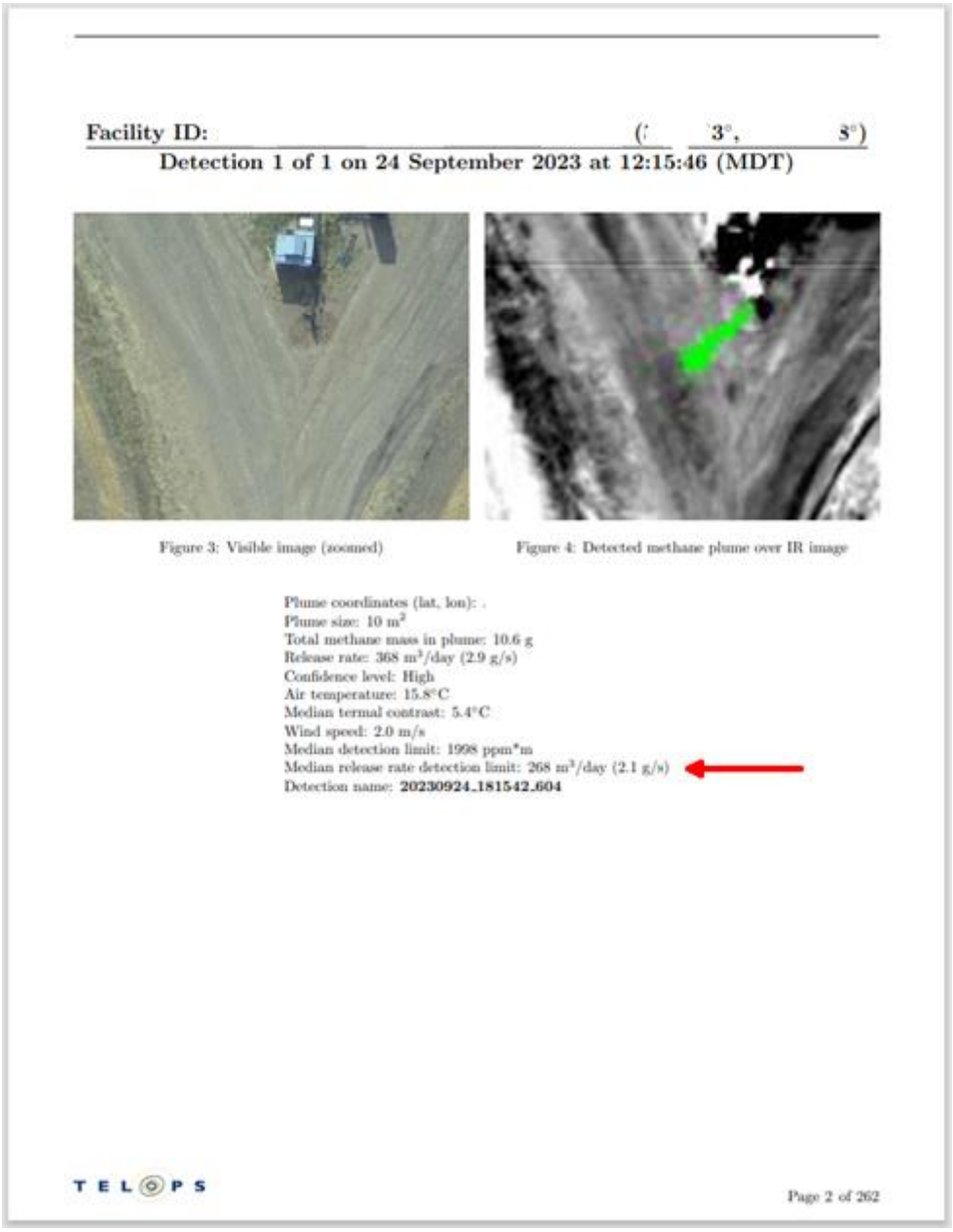

Facility ID: (3°, 3°)

Detection 1 of 1 on 24 September 2023 at 12:15:46 (MDT)

Figure 3: Visible image (zoomed)

Figure 4: Detected methane plume over IR image

Plume coordinates (lat, lon): .
Plume size: 10 m^2
Total methane mass in plume: 10.6 g
Release rate: 368 m^3/day (2.9 g/s)
Confidence level: High
Air temperature: 15.8°C
Median termal contrast: 5.4°C
Wind speed: 2.0 m/s
Median detection limit: 1998 ppm*m
Median release rate detection limit: 268 m^3/day (2.1 g/s)
Detection name: **20230924_181542_604**

TELOPS

Page 2 of 262

Figure 20: Sample detection report where the detection limit on the plume area is highlighted

In this section, we presented how the detection limit is handled, as its level depends on many variables and it is not a single value for the Hyper-Cam Airborne Mini. The detection limit calculation is part of our standard methane inspection processing, and its value is used during the inspection project to assess if the sites have been properly inspected and the values are presented in the final inspection report.

5.2.2 Experimental demonstration of the detection limit

The Hyper-Cam Airborne Mini has been tested under various flight and environmental conditions. Some of the tests were for detection performance demonstration and others were thorough tests of the system's capabilities using blind tests (semi-blind as the controlled release locations were known before the flight to properly prepare the flight plan for multiple flyovers). The results presented in this section are from a test which occurred during

the week of September 18th to 23rd, 2023 at CMC Brooks facility in Alberta (Canada) and financially supported by AMEP (Alberta Methane Emissions Program). During the 5 days of testing, 605 flyovers over 2 controlled release sites generated a total of 16883 measurements (hypercubes).

The system was intentionally tested under various conditions, to verify the detection limit model and demonstrate the actual detection performance. Methane controlled release rates was varied from 0.07 to 22.2 g/s (0.2 to 80 kg/h) including also "No Release" conditions. Wind speed varied from 1.7 to 4.1 m/s (6.1 to 14.8 km/h), flight speed varied from 46 to 90 knots, flight AGL from 250 to 410 m (820 to 1345 ft) and finally the thermal contrast varied from 0 to 15°C during that week at the end of September. One can expect higher thermal contrasts (>25°C) during summer conditions. Figure 21 presents the environmental conditions during the campaign and Figure 22, the flight conditions.

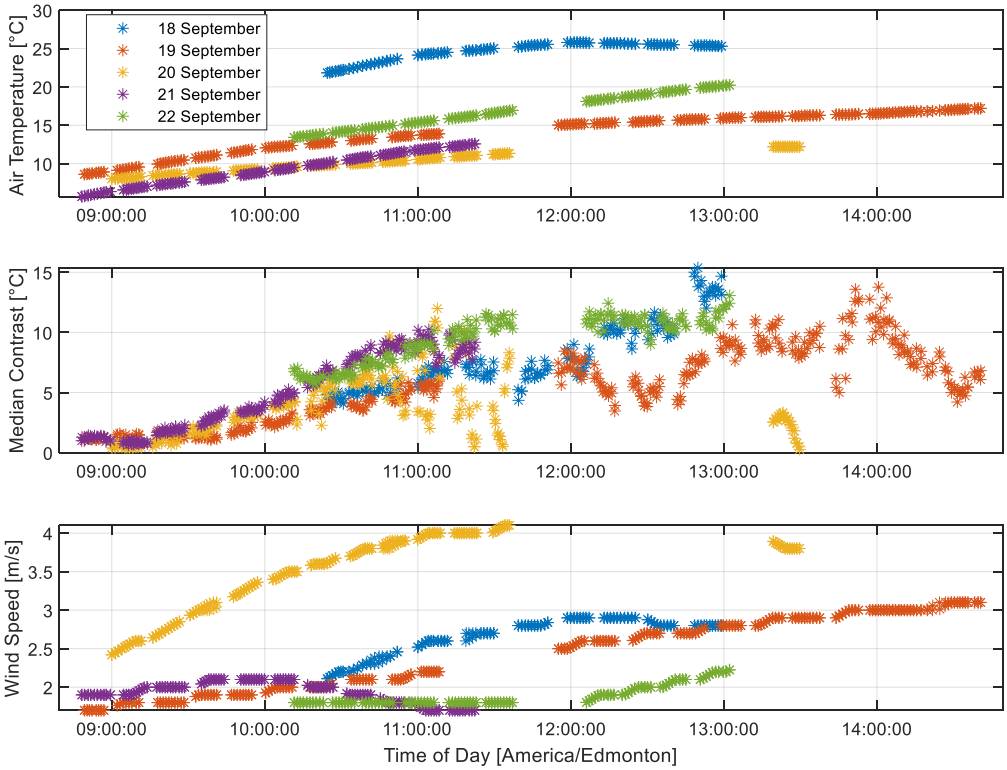

Figure 21: Measured air temperature, thermal contrast and wind speed values for every measurement during the test campaign

One can see that everyday, the thermal contrast was very low between 9h00 and 10h00 suggesting that for a normal inspection survey, it would be preferable to wait after 10h30 to get better contrasts. Nevertheless, this is perfect to test the detection limit (model and actual performance) at these low contrasts.

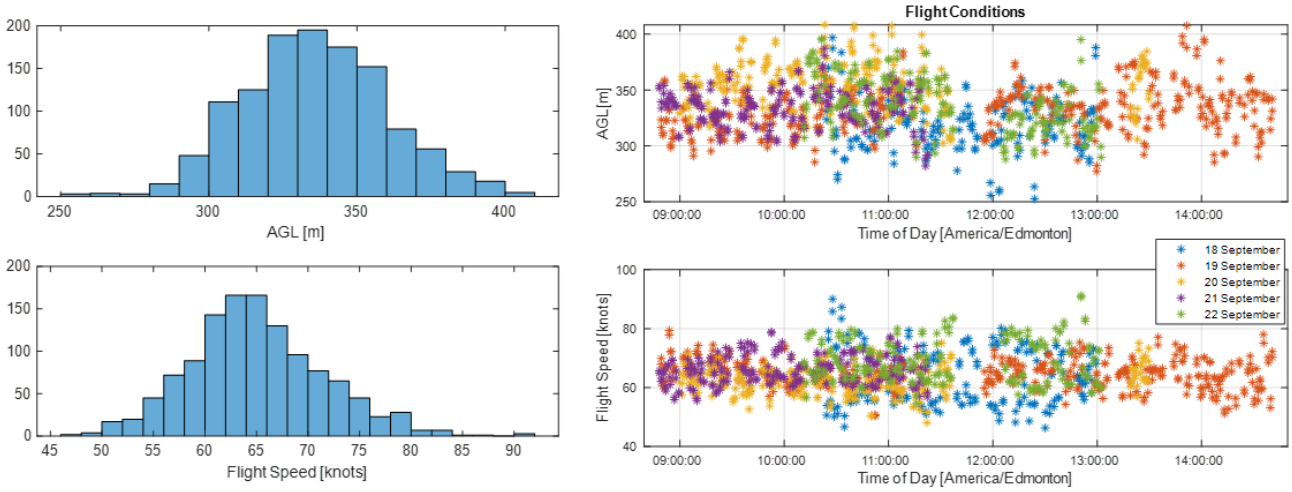

Figure 22: Flight conditions during the entire test campaign

Using our standard post-processing workflow, the detection limit is calculated for each acquired hypercube. These values obtained during the test campaign are plotted in Figure 23 as a function of the time of the day.

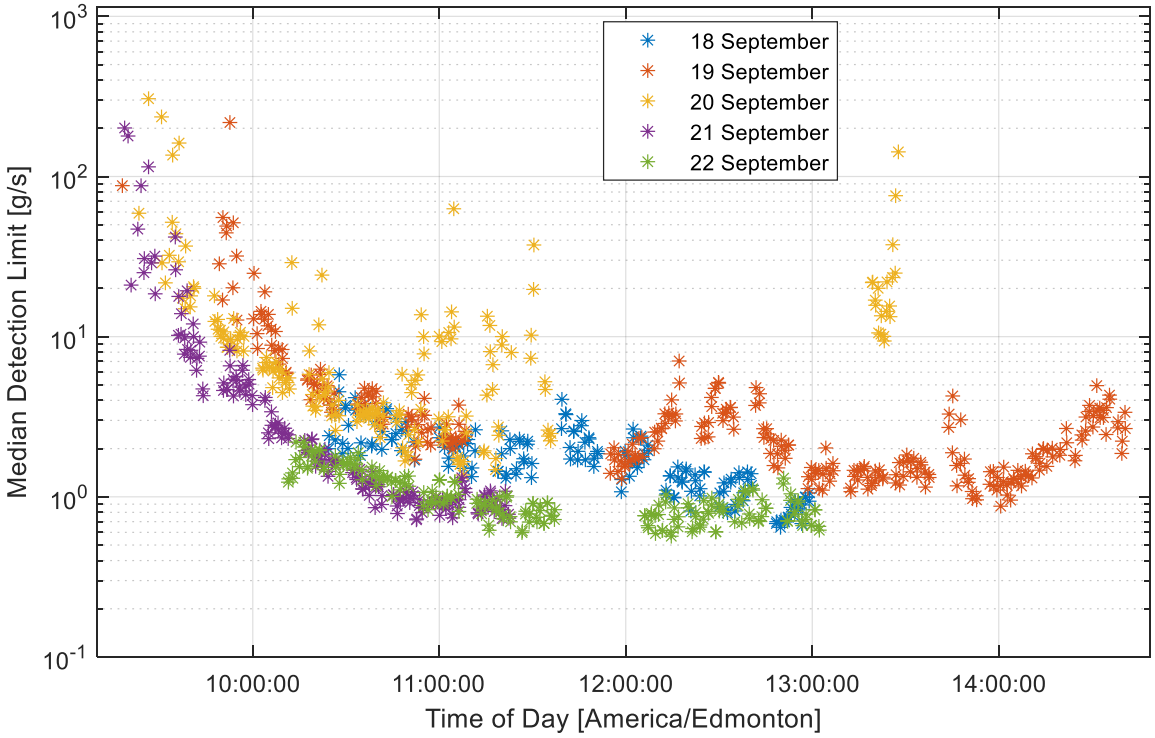

Figure 23: Calculated methane detection limit for all the measurements of the test campaign

One can clearly see the trend toward lower detection limit values from the beginning of the day to 10h30 local time. This is highly correlated with the thermal contrast presented in Figure 21. A wide range of detection limits has been tested, the best ones being around 0.6 g/s for that campaign.

In Figure 24 and Figure 25, we present the detection results for all the 16883 recorded hypercubes. For each hypercube, we place a data point (green being good detection, red being missed detection) where the x-coordinate is the calculated detection limit, and the y-coordinate is the actual controlled release rate.

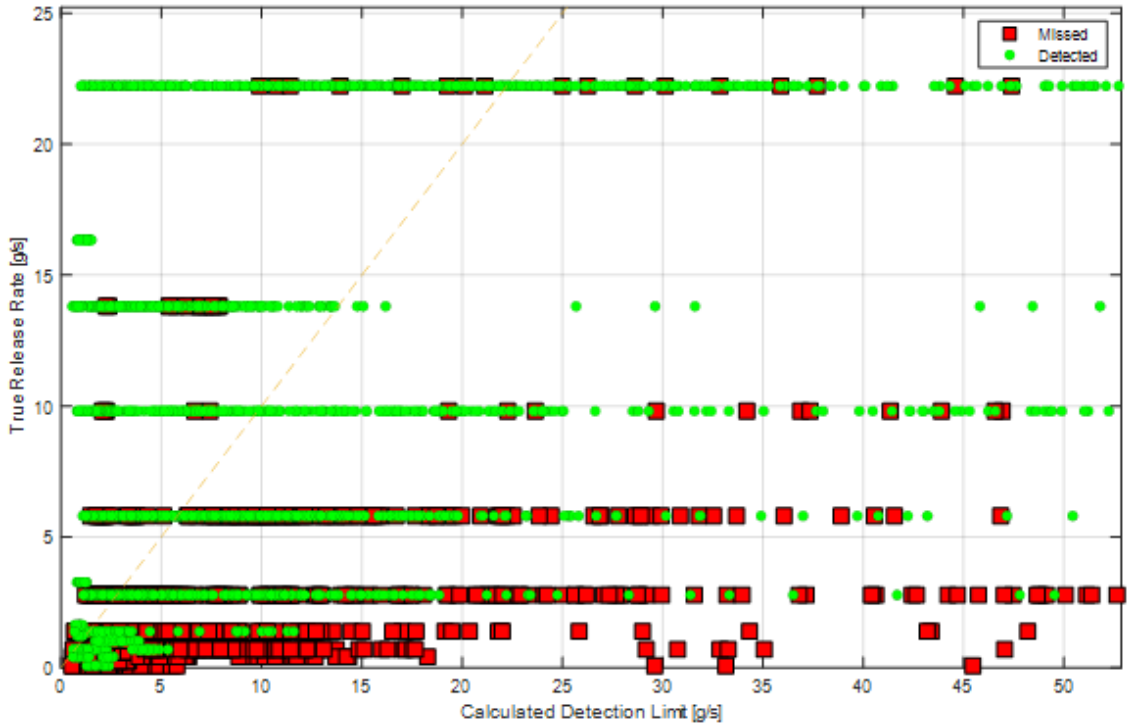

Figure 24: Hyper-Cam Airborne Mini Methane detection performance. Green points for true positive detections and red points for false negative detections (missed releases). The yellow dash line represents the case where the calculated detection limit is equal to the true rate of the controlled release.

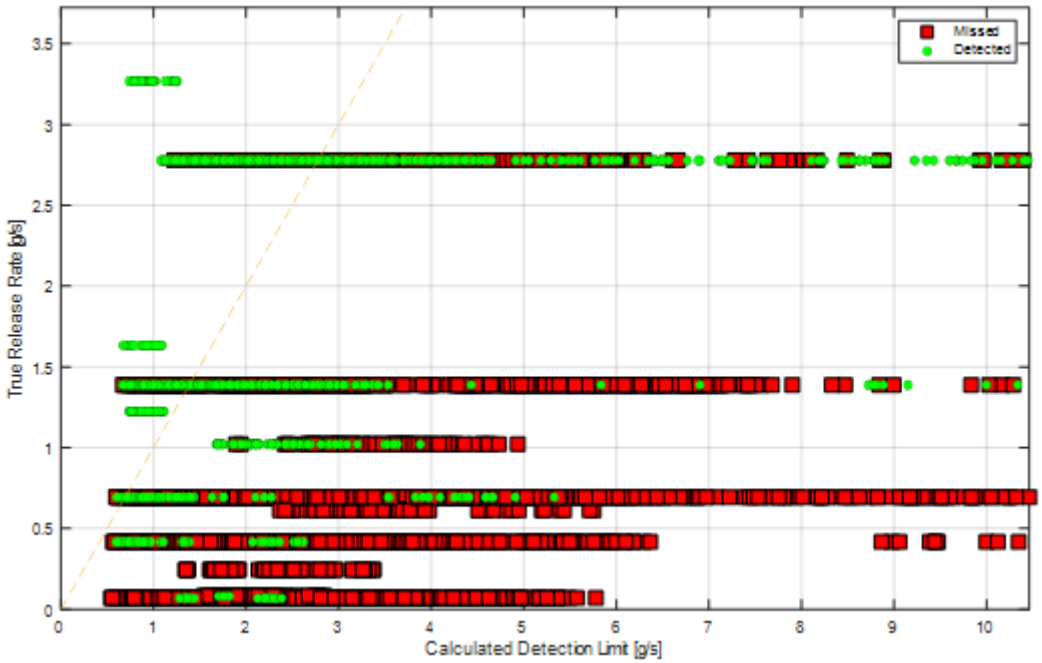

Figure 25: Hyper-Cam Airborne Mini Methane detection performance. Zoom on the lower left part of the plot presented in Figure 24.

From this dataset, we compute that we got 93% of detections when the release rate is above the calculated detection limit (data points above the yellow dash line), and 24% of detections when the release rate is below the

calculated detection limit. This probability of detection (PoD) gets higher when we consider only larger leak rates. This is shown in Figure 26 where we plot the PoD as a function of the release rate.

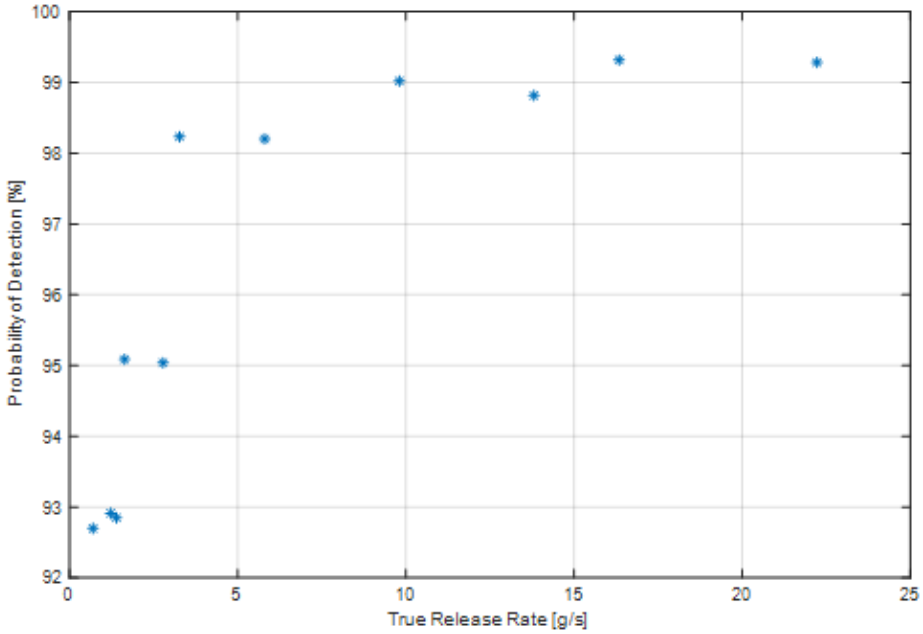

Figure 26: Probability of detection (PoD) as a function of the true release rate when the true release rate is above the calculated detection limit.

From this graph, we conclude that the probability of detecting a release of 5 g/s is 98% if this release rate is higher than the calculated detection limit. As implemented in the data processing workflow, the detection limit is calculated for each hypercube. This information is key to know the quality of the inspection and can be used as a conservative estimate of the 90% PoD detection limit, since it has been demonstrated to be the 92.7% PoD for release rates of 0.7 g/s (2.5 kg/hr) and above 98% PoD for release rates at and above 4 g/s (14.4 kg/hr).

5.2.3 Performance demonstration over snow-covered background

As mentioned earlier, the detection capability of the Hyper-cam Airborne Mini depends on the thermal contrast. It is worth to know that a snow-covered background produces good thermal contrast in the thermal infrared band where the Hyper-Cam Airborne Mini operates. Telops has previously achieved good results for methane detection under winter conditions (see Figure 27).

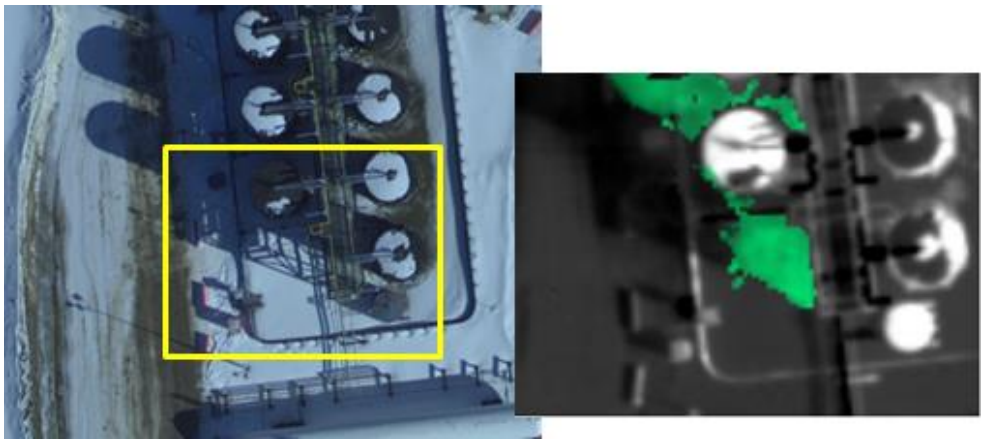

Figure 27: Example of methane release detection over snow-covered background

In this example from March 2023 in Canada, the air temperature is 4.1°C and the thermal contrast for the plume pixels over the snow-covered background goes from 1 to 10°C with a median value of 7°C as presented in Figure 28.

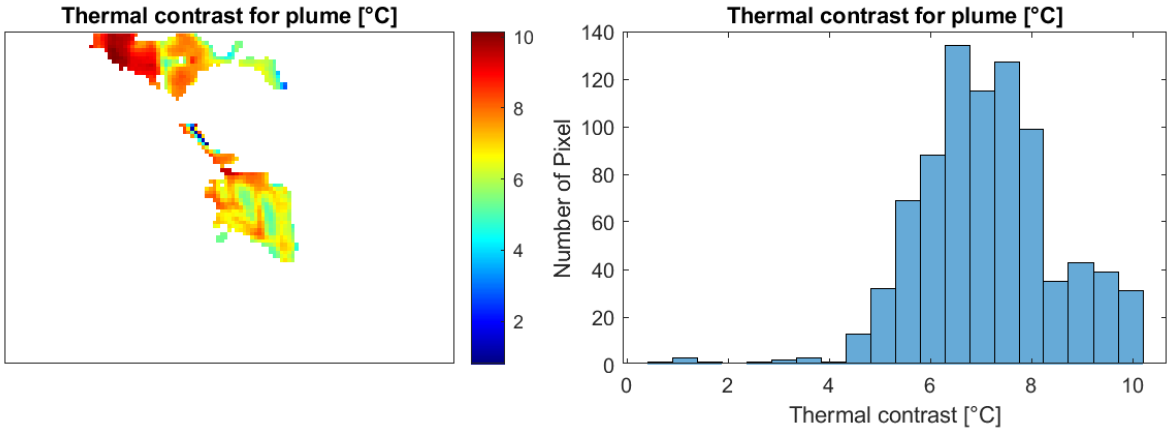

Figure 28: Thermal contrast for the plume pixels over a snow-covered background

In summary, Telops has developed and validated a detection limit model for the Hyper-cam Airborne Mini. The actual performance of the HCAM corresponds to the values obtained with the model. The detection limit has a dependence on the thermal contrast. The thermal contrast is computed for every hypercube allowing the determination of the actual detection limit for every measurement. Good thermal contrasts and good methane detection limits have been demonstrated for summer and winter conditions. Finally, nothing would prevent the use of the Hyper-Cam Airborne Mini to detect methane releases over water. Even if Telops never demonstrated the specific detection of methane over water, other gases have been detected over water with the Hyper-Cam (Puckrin, et al., 2021) since the physical principle remains the same, i.e. the molecule to be detected needs to have absorption in the spectral range of the hyperspectral camera.

6 Limitations

Section 5.2.1 presents in detail all the elements having an impact on the detection limit. Most of them have a small linear contribution factor, except for the thermal contrast. The detection limit exponentially increases for thermal contrasts below ~3°C. The management of the thermal contrast is important when using the HCAM, and

this is why the Telops' solution clearly exposes this value, in real-time during the inspection flight, and in all the post-flight reports. The other limitation of our remote sensing technology is the need for a clear line-of-sight of the methane cloud. The system does not receive any radiance signal from the ground when there is rain or snowfall. Similarly, if the methane cloud is hidden behind an object like a tree, an equipment, a roof or an infrastructure (below a bridge for example), it is not detectable.

7 References

Andrews David G. . An introduction to atmospheric physics (2nd éd ed.) [Book]. - Cambridge : Cambridge university press, 2010.

Bäumker Manfred & Heimes, F. New Calibration and Computing Method for Direct Georeferencing of Image and Scanner Data Using the Position and Angular Data of an Hybrid Inertial Navigation System [Journal] // Proceedings of OEEPE Workshop on Integrated Sensor Orientation. - 2002.

Foucher Pierre-Yves Real Time Gas Quantification Using Thermal Hyperspectral Imaging: Ground and Airborne Applications [Journal] // Phenomenology and Exploitation of Hyperspectral Sensing within NATO. - 2020.

Gordon I. E. The HITRAN2020 molecular spectroscopic database [Journal] // J. Quant. Spectrosc. Radiat. Transfer. - 2022. - p. 277.

Hodgkinson J, Sghan Q and Pride R D Detection of a simulated gas leak in a wind tunnel [Journal]. - [s.l.] : Measurement Science and Technology, 2006. - Vol. 17.

Idoughi R. Background radiance estimation for gas plume [Journal] // Journal of Spectroscopy, Hindawi Publishing. - 2016.

Manolakis Dimitris G. Comparative Analysis of Hyperspectral Adaptive Matched Filter Detectors [Journal] // Algorithms for Multispectral, Hyperspectral, and Ultraspectral Imagery VI. - 2000. - p. 4049.

Manolakis Dimitris G. Long-Wave Infrared Hyperspectral Remote Sensing of Chemical Clouds [Journal] // IEEE SIGNAL PROCESSING MAGAZINE. - 2014. - p. 120.

Puckrin Eldon [et al.] Remote Sensing of HNS using Longwave Infrared Hyperspectral Imaging [Book Section] // Remote Detection and Maritime Pollution: Chemical Spill Studies / book auth. Floch S.L. and Muttin, F.. - [s.l.] : Wiley, 2021. - Vol. chapitre 3.

Revercomb Henry E. [et al.] Radiometric calibration of IR Fourier transform spectrometers: solution to a problem with the High-Resolution Interferometer Sounder [Journal] // APPLIED OPTICS. - 1988.

Young S. J. An In-scene Method for Atmospheric Compensation of Thermal Hyperspectral Data [Journal] // J. Geophys. Res. Atmospheres Vol. 204,. - 2002. - pp. ACH 14-1 – ACH 14-20.

8 Appendices

Package 1	Description	Type
Inspection Statistics Report	Summary of the flight including timestamp of the flight. Number of scenes. Total inspection ground lines flown, total measurement length and	PDF

	graph about the weather and detection limits of each scene.	
Flight Path and Inspected Areas	KML file with the flight path and the median detection limit of each scene (can be open in google earth)	KML
Utilisation Summary	Information about the flight	Excel and .mat
Figures	A copy of the figures presented in the pdf report. Figures in the Matlab format and png.	.fig and .png

Package 2	Description	Type
Georeferenced IR broadband Image	Image of each scene	goetiff
Georeferenced Visible Image	Image of each scene	goetiff
Visible Image	Image of each scene	jpeg

Package 3	Description	Type
Detection Report	Report of each detection	excel
Detection Report	KML file with all the detection	KML
Detection image for each positive scene	Detection report	jpeg
Georeferenced IR broadband Image for each positive detection	Image of each scene with detection	geotiff
Georeferenced plume mask	plume mask of each scene with detection	geotiff
Georeferenced Visible Image for each positive detection	Image of each scene with detection	geotiff
Visible Image for each positive detection	Image of each scene with detection	jpeg
Zoomed in Visible Image (same size as the IR broadband)	Image of each scene with detection	jpeg
IR broadband Image with plume mask over it	Image of each scene with detection	jpeg
Summary report of each detection	Summary report of each scene with detection	png
Summary Inspection/Detection Report	A PDF report with all the campaign Inspection/Detection.	PDF